Resonant Enhancement of Magneto-Optical Activity Induced by Surface Plasmon Polariton Modes Coupling in 2D Magnetoplasmonic Crystals

Nicolò Maccaferri,[†] Xabier Inchausti,[†] Antonio García-Martín,[‡] Juan Carlos Cuevas,[§] Debashish Tripathy,[∥,⊥] Adekunle O. Adeyeye,[∥] and Paolo Vavassori*,[†,#]

[†]CIC nanoGUNE, E-20018 Donostia-San Sebastian, Spain

[‡]IMM-Instituto de Microelectrónica de Madrid (CNM-CSISC), Isaac Newton 8, PTM, Tres Cantos, E-28760 Madrid, Spain

[§]Departamento de Física Teórica de la Materia Condensada and Condensed Matter Physics Center (IFIMAC), Universidad Autónoma de Madrid, E-28049 Madrid, Spain
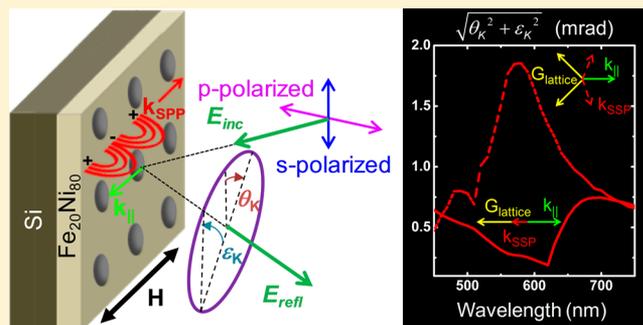
[∥]Information Storage Materials Laboratory, Department of Electrical and Computer Engineering, National University of Singapore, 117576 Singapore, Singapore

[#]IKERBASQUE, Basque Foundation for Science, E-48011 Bilbao, Spain

S *Supporting Information*

ABSTRACT: Magnetoplasmonic crystals are spatially periodic nanostructured magnetic surfaces combining the features of surface plasmon polariton excitation and magneto-optical tunability. Here we present a comprehensive experimental and theoretical work demonstrating that in magnetoplasmonic crystals the coupling of free space radiation to surface plasmon polariton modes in conjunction with the inherent magneto-optical activity, enable cross-coupling of propagating surface plasmon polariton modes. We have explored the consequences of this unique magnetoplasmonic crystal optical feature by studying the light reflected from a two-dimensional periodic array of cylindrical holes in a ferromagnetic layer illuminated at

oblique incidence and magnetized in the sample plane, namely, in the so-called longitudinal Kerr effect geometry. We observe that the magneto-optical spectral response arises from all the excitable surface plasmon polariton modes in the magnetoplasmonic crystal *irrespective* of the incoming light polarization. We show that this is a direct consequence of the magneto-optically mediated coupling of propagating surface plasmon polariton modes. We demonstrate that a large enhancement of the longitudinal Kerr effect is induced when special *noncollinear* surface plasmon polariton modes, which couple to both *p*- and *s*-polarized light, are resonantly excited. We show how the resonant enhancement of the Kerr effect can be set at desired radiation wavelengths and incidence angles by precise plasmonic band engineering achievable through the proper design of the magnetoplasmonic lattice structure. Our findings, besides clarifying the underlying physics that governs the peculiar magneto-optical properties of magnetoplasmonic crystals, open a path to the design of novel active metamaterials with tailored and enhanced magneto-optical activity.

KEYWORDS: *magneto-optical Kerr effect, surface plasmon polaritons, plasmonic crystal, magnetoplasmonics*

A surface plasmon polariton (SPP) is a transverse magnetic (*p*-polarized) electromagnetic wave, coupled to surface plasma charge oscillations, propagating at a metal/dielectric interface, which is evanescently confined in the perpendicular direction to the interface.[1,2] Similar to electrons in a crystal potential, the dispersion of SPP modes on a flat metal surface folds at the Brillouin zone boundaries to form a band structure when a periodic modulation of the metal surface is introduced, bringing about band-related concepts like phase and group velocity, photonic densities of states, and propagation anisotropy. This situation can be realized in one- or two-dimensional diffraction gratings, whose optical properties rely

on the generation of Bloch-like photonic band structures. These types of metal surfaces with periodic structures are called plasmonic crystals (PC) and are recognized as important elements in the field of plasmonics. While SPPs can couple to the free space using only impinging *p*-polarized light in a continuous film, efficient coupling of both *p*- and *s*-polarized (transverse electric polarized wave) light to SPP waves can be achieved through diffraction in metal surfaces with periodic arrangements of subwavelength scale structures.[3–8] This
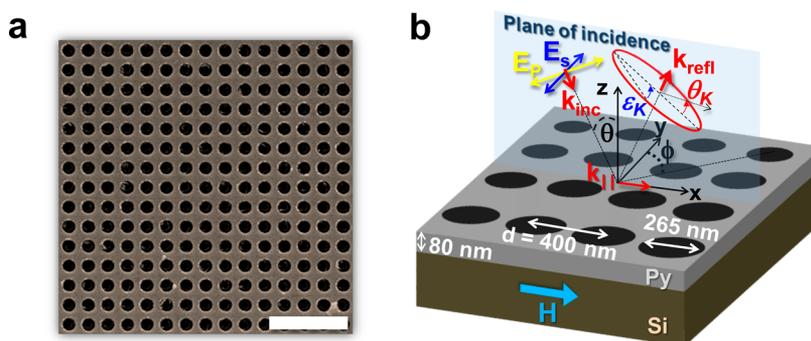
Figure 1. (a) SEM image of a portion of the 2D-MPC studied in this work. Scale bar 1.5μm. (b) Sketch of the 2D-MPC in the L-MOKE configuration.

property has been widely studied in the recent years in two-dimensional (2D) periodically patterned metal surfaces, named two-dimensional photonic crystals (2D-PC), for the design and optimization of SPP-light coupler devices. Remarkable examples are 2D-PC that make use of SPPs to give rise to extraordinary light transmission effects or to concentrate light in mirrors, wave guides, and cavities, whose enhanced light−matter interaction can be used in a broad variety of applications such as light modulators, devices for light energy harvesting, and biosensors.[9−15]

Intrinsic coupling of plasmonic modes through spin−orbit induced polarization conversion was recently demonstrated for localized surface plasmons in magnetic nanoantennas owing to their inherent magneto-optical (MO) activity.[16−18] In that case, desired light polarization behavior in transmission and/or reflection is achieved by tuning the relative phase of the excited and localized surface plasmons by precise design of the nanostructures (size and shape), with extremely promising applications to sensing and nano-optical devices.[19−21] Here we explore further the potential of the synergy between intrinsic MO-mediated polarization conversion and plasmon excitations by substituting localized with propagating surface plasmons in an archetypical 2D-magnetoplasmonic crystal (2D-MPC) made of periodic cylindrical holes in a ferromagnetic metallic layer. Perforated magnetic films implementing 2D-MPCs have been intensely studied in recent years, focusing in particular on the so-called Polar Magneto-Optical Kerr Effect, where the incident light wavevector and the magnetization vector are perpendicular to the sample plane.[22,24] In this case, the polarization state of the incident light is more conveniently described in terms of right and left circular polarization eigenmodes (pure p- and s-states are not defined), making this configuration more appropriate for exploiting optical properties of chiral systems. At oblique incidence, when p- and s-polarizations are defined, the great majority of the studies focused on the Transverse MOKE, which occurs for p-polarized incident light only and for in-plane magnetization perpendicular to the in-plane projection of the incidence radiation wavevector (namely, perpendicular to the incidence plane), driven by the notion that SPPs are efficiently excited by those p-polarized fields. In this MO configuration, polarization of reflected light remains unvaried and, thus, no MO-mediated polarization conversion is involved.[25−30] More recently, the remaining MOKE configuration, the Longitudinal-MOKE (L-MOKE, magnetization vector parallel to the in-plane projection of the incident radiation wavevector), was also considered.[31−33] In this MOKE configuration, polarization of the incident light can be either p or s. However, the case of s-polarized light received very limited

attention that, if considered at all, was more for the purpose of a systematic exploration of all MOKE configurations, rather than as a key configuration that could help unveiling the underlying physics and even less as a potentially exploitable case.

Here we show, by performing dedicated experiments and theoretical simulations, that L-MOKE configuration allows a more extensive exploitation of SPP modes band structure in 2D-MPCs. In particular, we demonstrate that the possibility to excite with both p- and s-polarized light noncollinear (wave-vectors of the incident light and of the SPP not parallel) and bidirectional SPPs (twofold degenerate bands with SPPs propagating in different directions) can be used for the resonant enhancement of the MO response. The underlying mechanism relies on the coupling between such SPPs enabled by the MO-induced polarization conversion upon meeting specific conditions (light incidence angle and wavelength, 2D-MPC orientation), which are presettable by design (array spacing and symmetry). We show that the most interesting features observed in the L-MOKE spectra, namely, appearance of plasmon-induced resonant line shapes and notable MO enhancement effects, arise from the resonant interference between reflected light due to SPP modes directly excited by the incident light and light re-emitted by the MO-induced SPP modes, whose polarization is perpendicular to that of the incident field. Besides providing a deeper understanding of light matter coupling in 2D-MPCs, our results disclose how to exploit the SPPs coupling activated by the MO-mediated polarization conversion via plasmonic band engineering leading to enhancement of MO signals at desired wavelengths.

RESULTS AND DISCUSSION

The system studied in this work is a 2D-MPC made of subwavelength holes in a continuous film, 80 nm thick, of Permalloy ($Ni_{80}Fe_{20}$ or Py) on a Si substrate arranged on a square lattice.[30] A SEM image of a portion of the system is shown in Figure 1a. The lattice constant is 400 ± 5 nm, and the diameter of the holes is 265 ± 5 nm. The optical reflectivity of the system, namely, the ratio between the intensity of the reflected and incident electric fields, was measured using angle-resolved reflectometry, where the incident light is either s- or p-polarized. Upon the application of an external in-plane magnetic field H parallel to plane of incidence, the so-called L-MOKE configuration, a MO activity (MOA) is induced in the system, and the reflected light becomes elliptically polarized (Figure 1b). In other words, the application of an external static magnetic field that fully magnetizes the sample, induces optical
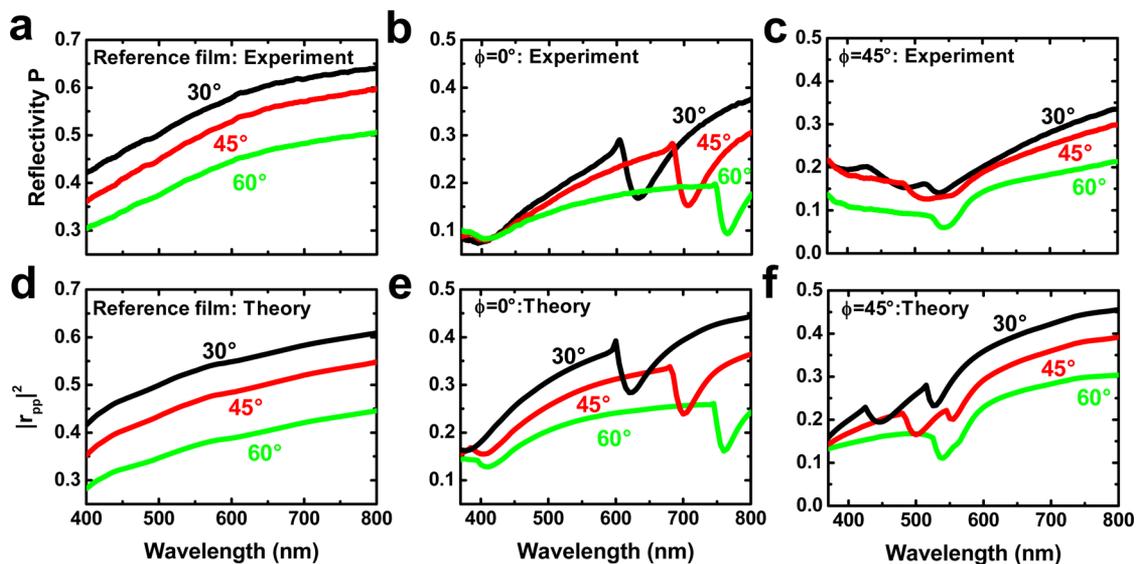
Figure 2. *p*-polarized incident light case. Three angles of incidence: black lines − θ = 30°, red lines − θ = 45°, green lines − θ = 60°. Reflectivity spectra of the reference film (a), of the 2D-MPC at ϕ = 0° (b) and at ϕ = 45° (c). Calculated reflectivity of the reference film (d), of the 2D-MPC at ϕ = 0° (e) and at ϕ = 45° (f).
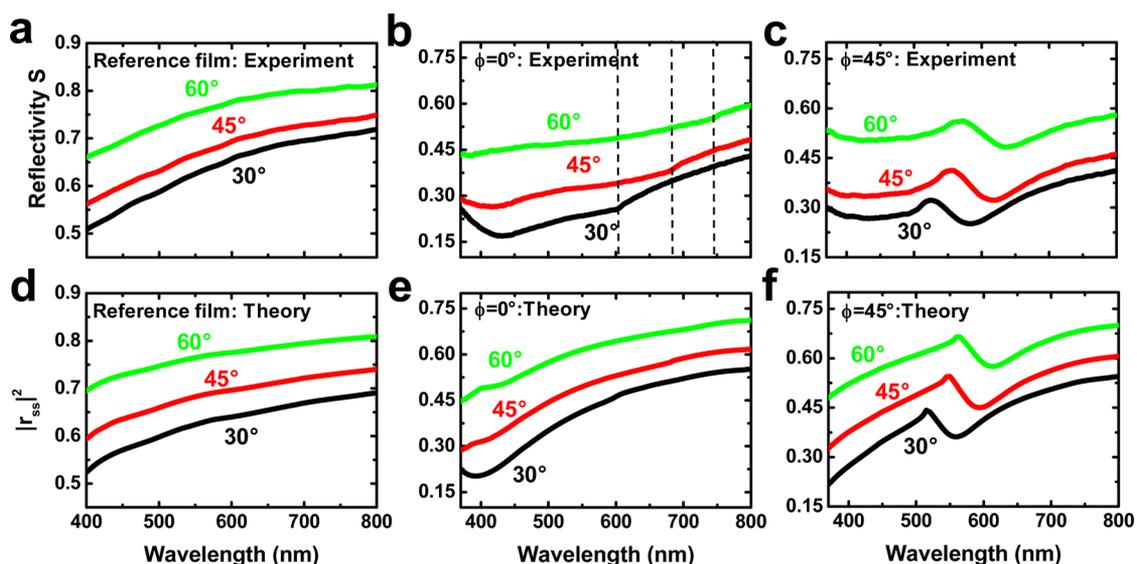

Figure 3. *s*-polarized incident light case. Black lines − θ = 30°, red lines − θ = 45°, green lines − θ = 60°. Reflectivity spectra of the reference film (a), and of the 2D-MPC at ϕ = 0° (b) − dashed lines indicate the position of the Rayleigh's anomalies − and at ϕ = 45° (c). Calculated reflectivity of the reference film (d), and of the 2D-MPC at ϕ = 0° (e) and at ϕ = 45° (f).

nonreciprocity in the material, namely, a coupling between *s*- and *p*-modes.[31]

In the first place, we investigated the plasmonic band structure of our 2D-MPC by performing angular resolved optical reflectivity experiments in the visible and near-infrared spectral range, and by numerical simulations using an adapted scattering matrix method (SMM) approach able to describe both the optical and MO effects in periodically patterned multilayered systems.[34] We used as input elements for the numerical simulations tabulated experimental optical and MO dielectric constants of Py,[35] which are plotted in Supporting Information, Figure S1. In Figures 2 and 3 we report representative reflectivity spectra measured and calculated for both *p*- (Figure 2) and *s*-polarization (Figure 3) for three different angles of incidence (θ = 30°, 45°, and 60°) and for the two high-symmetry azimuthal configurations (ϕ = 0° and 45°).

In Figure 2a we display the measured reflectivity spectra of a reference continuous film of Py, which was deposited simultaneously during the fabrication of the 2D-MPC, for the same values of θ. The measured reflectivity is defined as the ratio between the intensity of the reflected and incident electric field. No particular features are present in the reference film spectrum that could be ascribed to coupling of incident light to SPP modes in the explored experimental range. This is what is expected for a continuous metallic film where the dielectric medium hosting the incoming wave and that is in contact with the metal is air. In this case, it is well-known that the in-plane projection of the wavevector of the incident light $k_\parallel(\lambda)$ cannot couple to any SPP mode, since $k_\parallel(\lambda) < k_{SPP}(\lambda) = 2\pi((\varepsilon\varepsilon_m)/(\varepsilon + \varepsilon_m))^{1/2}/\lambda$, where ε is the dielectric function of the metal and ε_m is the dielectric function of the dielectric medium (for air ε_m = 1).[1,2] The dispersion relation of the plasmon wavevector, as
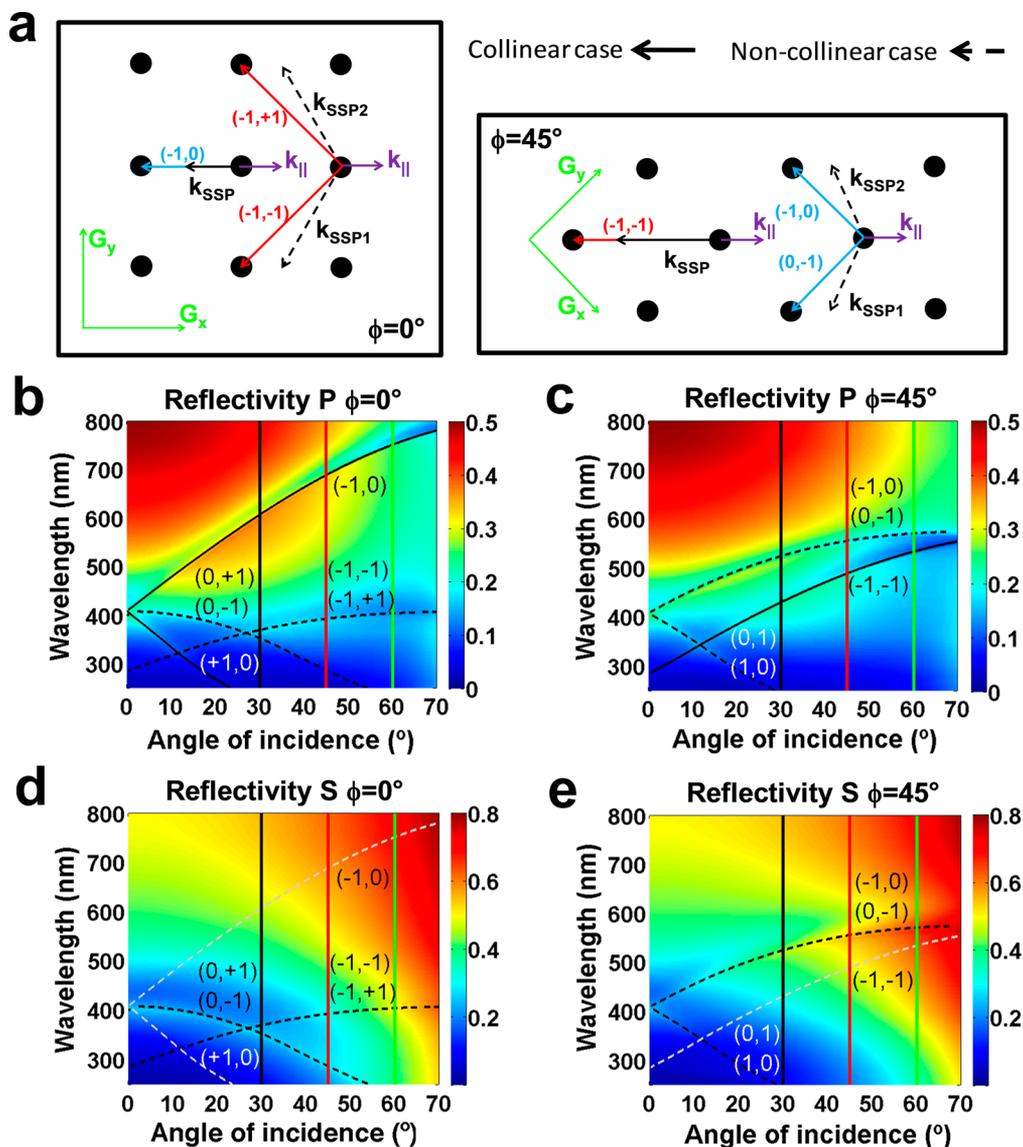
Figure 4. . (a) Left panel: sketch of collinear and non-collinear SPP modes in the reciprocal space for $\phi = 0°$. Right panel: sketch of collinear and noncollinear SPP modes in the reciprocal space for $\phi = 45°$. (b) Reflectivity of the system for p-polarized light and $\phi = 0°$. The vertical solid lines indicate the three angles of incidence studied experimentally. The black solid lines indicate the collinear modes, whereas the black dashed lines indicate the noncollinear modes. (c) Reflectivity of the system for p-polarized light and $\phi = 45°$. (d) Reflectivity of the system for s-polarized light and $\phi = 0°$. (e) Reflectivity of the system for s-polarized light and $\phi = 45°$. The grey dashed lines indicate the forbidden collinear modes for the s-polarization case. All the lines indicating allowed/forbidden modes are calculated using eq 1. The different colours (black or white) used for labelling the modes is just for improving their legibility.

well as the propagation length of the SPP modes, in a continuous Py film, are plotted in Supporting Information, Figure S2.

In Figure 2b we plot the optical spectra of our 2D-MPC measured at $\phi = 0°$ for the same values of θ. In this case, we notice two clear spectral dips (Wood's anomalies, WAs) brought about by the introduction of periodicity, which are the signature of light coupling to a SPP mode. WAs in the reflectivity spectra reveal the appearance of additional channels of light energy flux along the sample surface due to resonant excitation of SPP waves. We observe a slightly θ-dispersive WA in the range 380−410 nm, weakly red-shifting when increasing θ. A more θ-dispersive WA, also red-shifting as θ increases, is observed in the range 600−800 nm. In Figure 2c we plot the optical spectra measured at $\phi = 45°$ and for the same values of θ that clearly display two separated WAs at $\theta = 30°$ (black line),

which progressively get closer to each other as θ is increased (red line $\theta = 45°$ and green line $\theta = 60°$). These experimental results agree well with our numerical calculations performed using SMM, where the reflectivity was calculated as $|r_{\text{pp(ss)}}|^2$, with $r_{\text{pp(ss)}}$ being the complex Fresnel coefficients of the reflected light for $p(s)$-polarized light (see Figures 2d−f).

In Figure 3a we show the measured reflectivity spectra for s-polarized incident light of the reference continuous film for the same values of θ. Also in this case, no particular features traceable to the excitation of SPP modes are present in the reference film spectrum. In Figure 3b the optical spectra of the 2D-MPC measured with s-polarized light and at $\phi = 0°$ for the three selected values of θ do not display the resonant excitation of any SPP mode in the spectral range 600−800 nm at variance with the p-polarization case: only a small kink due to the occurrence of a Rayleigh's anomaly is visible (see the vertical

dashed lines in Figure 3b). For this particular sample orientation, the spectra show a weak WA in the range 380−410 nm. The shallow dip produced by the WA in the spectra is slightly red-shifted and broader with respect to that observed using p-polarized light. These broadening and red-shifting of WAs excitable with both polarizations, when the light polarization is changed from p to s, has been already observed in PCs.[4,5]

In Figure 3c, we display the reflectivity spectra of the 2D-MPC for s-polarization, $\phi = 45°$ and for the same values of θ. Now, the s-polarized incident light can resonantly excite only one SPP mode in the wavelength range 500−650 nm, whose θ-dispersive behavior displayed by the corresponding WA is the same as that of the WA appearing at longer wavelength in the same spectral range using p-polarized light. Again, the experimental results are in excellent agreement with numerical calculations of the reflectivity coefficients using SMM (see Figure 3d−f).

In order to identify the excited SPP modes that correspond to the WAs observed in the spectra, we calculated the plasmonic dispersion bands using a perturbative approach valid in the limit of vanishing small holes.[9] Within the perturbative approach, the SPP modes of the 2D-MPC can be expressed as linear combination of the continuous film modes and the photonic bands are obtained from k-conservation relationship, in which the contribution of the diffraction grating is included:

$$|k_{SPP}|^2 = (k_x + m\mathbf{G}_x)^2 + (k_y + n\mathbf{G}_y)^2 \qquad (1)$$

where $k_x = k_0 \sin\theta \cos\phi$ and $k_y = k_0 \sin\theta \sin\phi$ are the x and y projections of the incident light wavevector k_0, respectively, $\mathbf{G}_x = 2\pi/d_x$ and $\mathbf{G}_y = 2\pi/d_y$ are the x and y components of the lattice reciprocal vector $\mathbf{G}$, and n and m are integer numbers. The values of the lattice parameter along x and y directions are labeled with d_x and d_y, respectively. Of course, in the case of a square lattice investigated here, $d_x = d_y = d$.

Two different kind of modes are identified and sketched in Figure 4a: (i) plasmonic bands with $k_\parallel \parallel \mathbf{G}$ and, thus, $\parallel$ to k_{SPP} (collinear case); each band of this type corresponds to a directional SPP wave, namely, a SPP wave propagating with k_{SPP} either parallel or antiparallel to $k_\parallel$; (ii) plasmonic bands for which $k_\parallel$ is *not* parallel to $\mathbf{G}$ and, thus, neither to k_{SSP} (noncollinear case). In the noncollinear case, the plasmonic band originates from two degenerate SPP waves propagating in different directions (k_{SPP1} and k_{SPP2}, with $|k_{SPP1}| = |k_{SPP2}|$). Hereafter, the indexes pair (m, n) of the $\mathbf{G}$ involved in the coupling is used to label the plasmonic bands for clarity. The simple perturbative approach used to identify the bands does not take into account neither of the dimensions of the holes nor of the field symmetry-related selection rules that determine the cross section of the light-SPP coupling.[5,9,20,31] In spite of this limitation, the plasmonic dispersion bands calculated using the perturbative approach correlate well to the salient features in the 2D reflectivity intensity maps obtained from numerical simulations using the SMM technique, in the angles range 0−70° for p-and s-polarization (Figure 4b,c and d,e, respectively) and for the two azimuth angles investigated ($\phi = 0°$ in Figure 4b,d, and $\phi = 45°$ in Figure 4c,e). Solid and dashed black lines in Figure 4b−e identify plasmonic bands for collinear and noncollinear modes, respectively. Plasmonic bands, of either type, that are not excitable by a specific polarization are highlighted by gray dashed lines. It is worth stressing that the

SMM approach computes the light-SPP coupling cross section taking into account the symmetry selection rules as well as the holes-size effect. Regarding the noncollinear case, it is important to mention that the two SPP waves propagating with wavevectors k_{SPP1} and k_{SPP2} determined with the perturbative approach are coupled due to their degeneracy. As a consequence, the noncollinear bands actually correspond to the dispersion relation of two coupled SPP modes that can be described as the superposition of the two SPP waves with k_{SPP1} and k_{SPP2}. The symmetries of the resulting coupled SPP modes impose selection rules on their coupling to linearly polarized free-space plane waves. Thus, each coupled mode can only be excited by free-space radiation with a specific polarization, either p or s.[9] The vertical colored lines in Figure 4b−e indicate the three values of θ of the experimental spectra shown in Figures 2 and 3, namely, 30°, 45°, and 60°. The intersection between these lines and the dispersion bands allow us to precisely correlate the SPP modes excited to the Wood's anomalies observed in the spectra and discussed in Figures 2 and 3.

A first result from the inspection of Figure 4b,c is that p-polarized light can excite SPP modes of both kinds, collinear and noncollinear, although with different efficiency; on the contrary, s-polarized light can excite only SPP modes of the second kind (noncollinear case, black dashed lines). In the case of p-polarized light and $\phi = 0°$ (Figure 4b), the intersections with the vertical lines reveal that the excited SPP modes observed experimentally in Figure 2 are the mode (−1,0) in the range 600−800 nm (collinear case, black solid line), and one of coupled modes originated by the (−1,+1) and (−1,−1) SPP waves in the range 380−410 nm (degenerate plasmonic bands, noncollinear case, black dashed line). For $\phi = 45°$ (Figure 4c), the intersection indicates that the incoming p-polarized light couples to a coupled mode arising from the two degenerate directional SPP waves (−1,0) and (0,−1) (noncollinear case for this orientation of the array, black dashed lines). The other SPP mode excited is the (−1,−1), which for this orientation of the sample corresponds to a collinear case (solid black line).

In the case of s-polarized light and for $\phi = 0°$ (Figure 4d), the plasmonic band (−1,0) is not accessible due to selection rules arising from the symmetries of the collinear SPP modes,[9] and only a coupled mode arising from the SPP waves in the degenerated (−1,+1) and (−1,−1) plasmonic bands can be excited at 400 nm (noncollinear case). For $\phi = 45°$ (Figure 4e), s-polarized light can couple only to a coupled mode due to the two SPP waves in the degenerate (−1,0) and (0,−1) plasmonic bands (noncollinear case for this orientation of the array, black dashed line in the color map) alike in the p-polarization case. In this case, the coupling of the s-polarized light to the SPP mode in the (−1,−1) plasmonic band, corresponding to the collinear case for this orientation of the sample, is prevented by symmetry selection rules (gray dashed line).

To summarize and conclude this discussion, we highlight that for both $\phi = 0°$ and $\phi = 45°$ there are collinear SPP modes that can be excited only with p-polarized light, while there are noncollinear and degenerate SPP coupled modes that can be excited by either s- or p-polarized light: for $\phi = 0°$ and in the explored wavelength range, these latter type of SPP coupled modes arise from the superposition of SPP waves whose dispersion is described by the degenerate (−1,+1) and (−1,−1) plasmonic bands, while for $\phi = 45°$ they result from the superposition of SPP waves in the degenerate (−1,0) and (0,−1) bands.

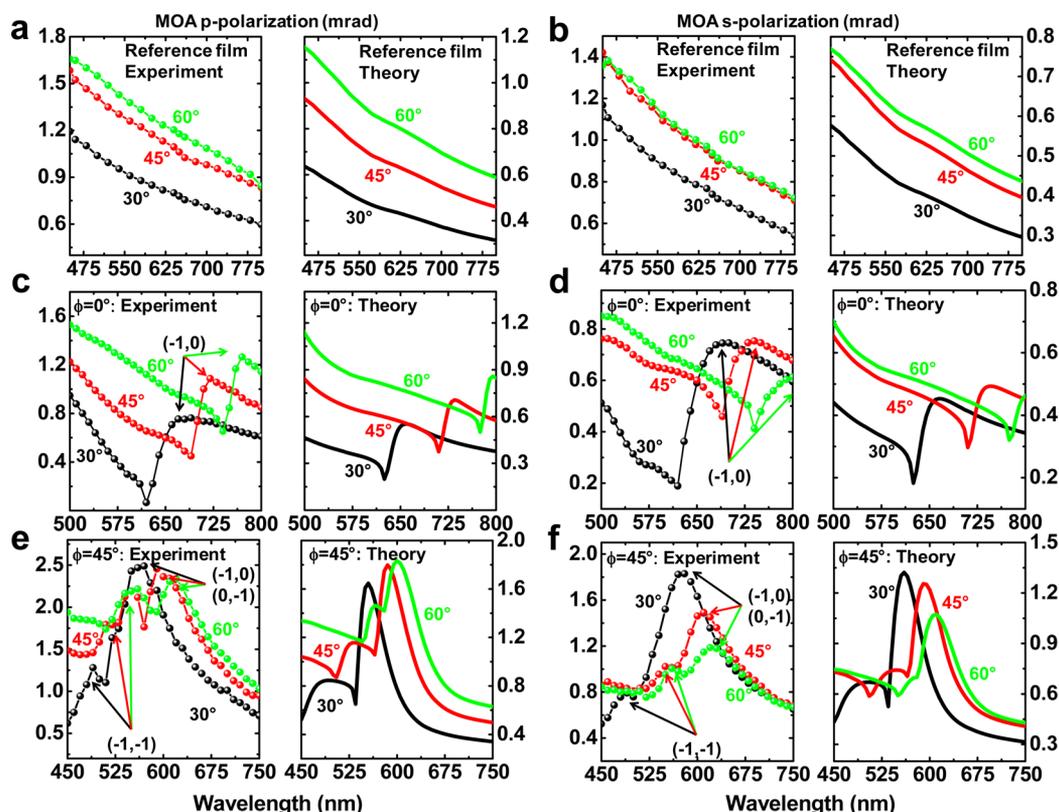**Figure 5.** MOA of the 2D-MPC for three angles of incidence: black lines − $\theta = 30°$, red lines − $\theta = 45°$, green lines − $\theta = 60°$. Experiments (left panels) and calculations (right panels). (a) MOA of the reference film with p-polarized light. (b) MOA of the reference film with s-polarized light. (c) MOA of the 2D-MPC with p-polarized light at $\phi = 0°$. (d) MOA of the 2D-MPC with s-polarized light at $\phi = 0°$. (e) MOA of the 2D-MPC with p-polarized light at $\phi = 45°$. (f) MOA of the 2D-MPC with s-polarized light at $\phi = 45°$.

We then investigated the interplay between MO activity and the plasmonic band structure of our 2D-MPC through L-MOKE by applying an in-plane static magnetic field H to magnetically saturate the sample along a direction parallel to the in-plane projection of the incidence radiation wavevector (see Figure 1b). Figure 5 shows the experimental and theoretical L-MOKE spectra of the reference film and of the 2D-MPC for the same three values of θ and for the two orientations of ϕ of the reflectivity spectra shown in Figures 2 and 3. To be precise, Figure 5 displays the spectra of the MOA of the systems at saturation, defined as $(\theta_K^2 + \varepsilon_K^2)^{1/2}$, where θ_K and ε_K are the H-field induced Kerr rotation and ellipticity polarization angles, respectively.[28]

In the same manner as for the reflectivity curves, the MOA of the reference continuous film does not display any particular feature for neither light polarization states that can be traced back to the resonant excitation of SPP modes (Figure 5a,b). In the case of the 2D-MPC, resonances with an asymmetric line shape are clearly observed in the spectra shown in Figure 5c−f. The most striking result is the similarity of the spectral line shapes measured with s- and p-polarized light, which carry signatures of *all* the excitable SPP modes discussed above, *irrespective* of the incident light polarization.

Given the previous discussion on Figure 4, namely, that p-polarized light can couple to all modes present in the selected spectral range, while s-polarized one only to a subset of them, this result is unexpected and points to the fact that, through the intrinsic MO-induced polarization conversion, *all* the excitable SPP modes contribute to determine the MOA. More precisely, for $\phi = 0°$ we observe a deviation, from the continuous film

response, of the MOA for both polarizations (Figure 5c,d), which corresponds to the excitation of the collinear SPP mode $(-1,0)$ in the wavelength range 600−800 nm. This mode cannot couple directly to s-polarized incident light, as discussed above. Therefore, it must appear in the MOA measured with s-polarized light because it is excited via the conversion between s- and p-polarizations provided by the intrinsic MO properties of the 2D-MPC. Moreover, this polarization conversion effect seems to be very efficient as the spectral intensities of the plasmon-induced features are very similar for the two polarizations, although in the p-polarization case the mode $(-1,0)$ is excited directly by the incident light, while in the s-polarization case it is excited via the MO-induced polarization conversion. The MO-mediated coupling between polarized light and SPP modes is further corroborated in the even more interesting case of $\phi = 45°$ (Figure 5e,f). In this case, we see signatures of all the possible modes in the explored spectral range for both light polarizations. These modes are the $(-1,-1)$ collinear case, and the two degenerate coupled modes arising from the $(-1,0)$ and $(0,-1)$ noncollinear SPP waves, yielding to a plasmon-induced spectral shape in the MOA responses. At variance with the previous case of $\phi = 0°$, now we also see a clear and remarkable enhancement of the MOA with respect to the continuous film in the wavelength range 550−650 nm, up to a factor ~2.5 in the case of p-polarization. The individual polarization parameters, rotation and ellipticity, show the same enhancement compared to the film case (see Supporting Information, Figure S3 for the case $\phi = 45°$ and $\theta = 30°$, and Supporting Information, Figure S4 for the intensity maps of the ratio between the MOA of the 2D-MPC and that of the
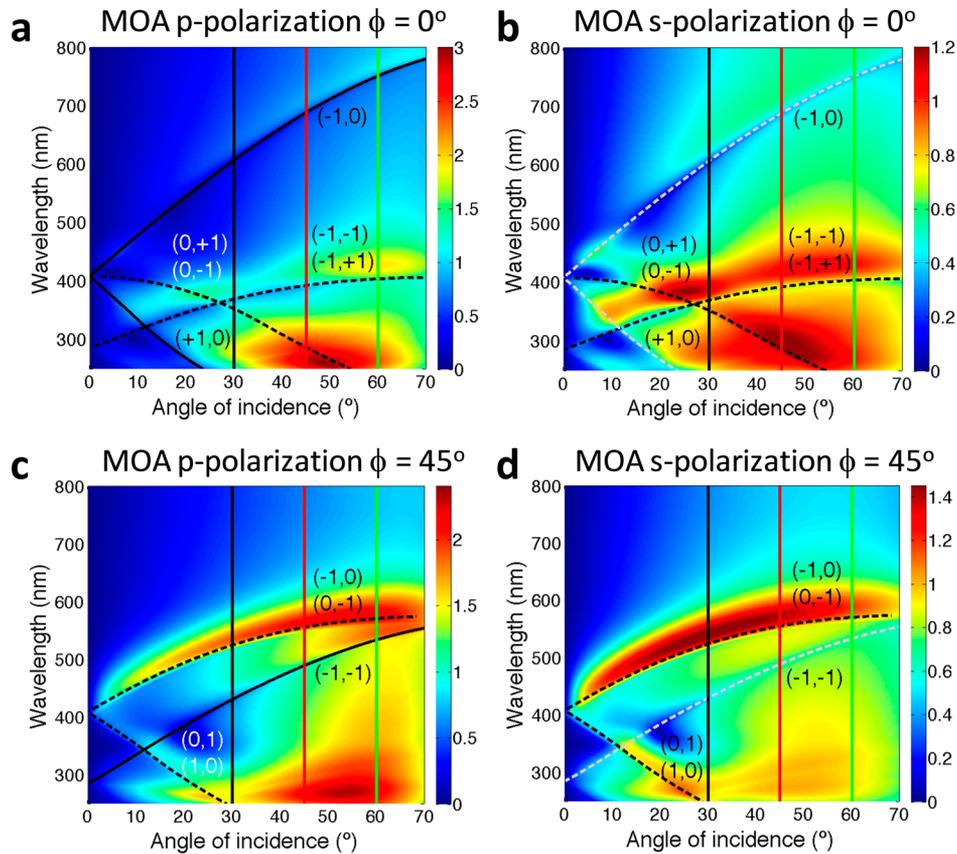
Figure 6. Calculated MOA, in mrad, of the 2D-MPC. (a) p-polarized light and $\phi = 0°$. (b) s-polarized light and $\phi = 0°$. (c) p-polarized light and $\phi = 45°$. (d) s-polarized light and $\phi = 45°$. The black solid lines indicate the collinear modes, whereas the black dashed lines indicate the noncollinear modes. The grey dashed lines indicate the forbidden collinear modes for the s-polarization case. All the lines indicating allowed/forbidden modes are calculated using eq 1. The different color (black or white) used for labelling the modes is just for improving their legibility.
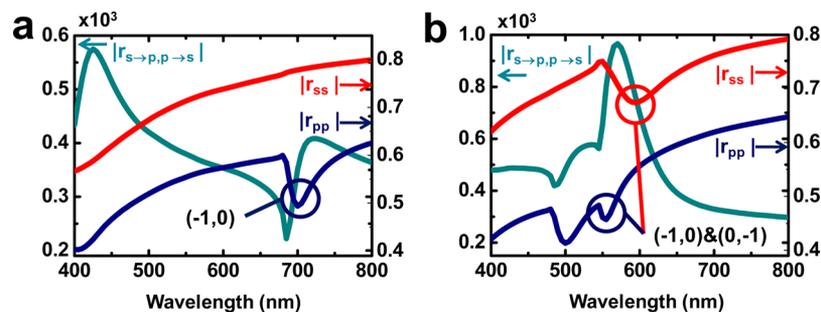

Figure 7. (a) Calculated absolute values of the reflection coefficients and of the MO-induced polarization conversion reflection coefficients. (a) $\phi = 0°$ and $\phi = 45°$, with highlighted the WA corresponding to the excitation of the collinear mode $(-1,0)$ (dark blue circle), excitable with p-polarized light only. (b) $\phi = 45°$ and $\theta = 45°$, with highlighted the WAs corresponding to the excitation of the noncollinear modes $(-1,0)/(0,-1)$ (dark blue and red circles), excitable with both s- and p-polarized light.

continuous film). This remarkable enhancement results from the possibility of the *simultaneous excitation* of the two degenerate coupled modes arising from the noncollinear SPP waves $(-1,0)$ and $(0,-1)$ with both s- and p-polarized incident light. The experimental data are again fully supported by the MOAs spectra calculated using the SMM approach, which are shown in Figure 5.

The conclusions above are further confirmed by the MOA spectral intensity maps for the two polarizations calculated in the spectral range 250–800 nm, θ range 0–70°, and for ϕ equal to 0° and 45° shown in Figure 6. For each azimuth angle ϕ, the maps are identical, apart from their slightly different intensity, and clearly show signatures of all the excitable modes,

independent of the light polarization, proving that the MO coupling enables the activation of modes in the magneto-optics that are forbidden (collinear case) for the s-polarization. The difference in the intensities between the MOA with p- and s-polarization is merely due to the higher pure optical reflectivity for s-polarization as compared to p-polarization (compare panels of Figures 2 and 3). This is easy to understand from the definition of the MOA, which reads $\text{MOA}_{s(p)} = |r_{s \to p}(r_{p \to s})|/|r_{ss}(r_{pp})|$. Thus, the fact that $|r_{ss}|$ is larger than $|r_{pp}|$ naturally explains why the MOA for s-polarized light is less intense than that for p-polarized light.

Indeed, the spectra in Figure 7a for $\phi = 0°$ and $\theta = 45°$ (see also complete spectral intensity maps in Supporting informa-
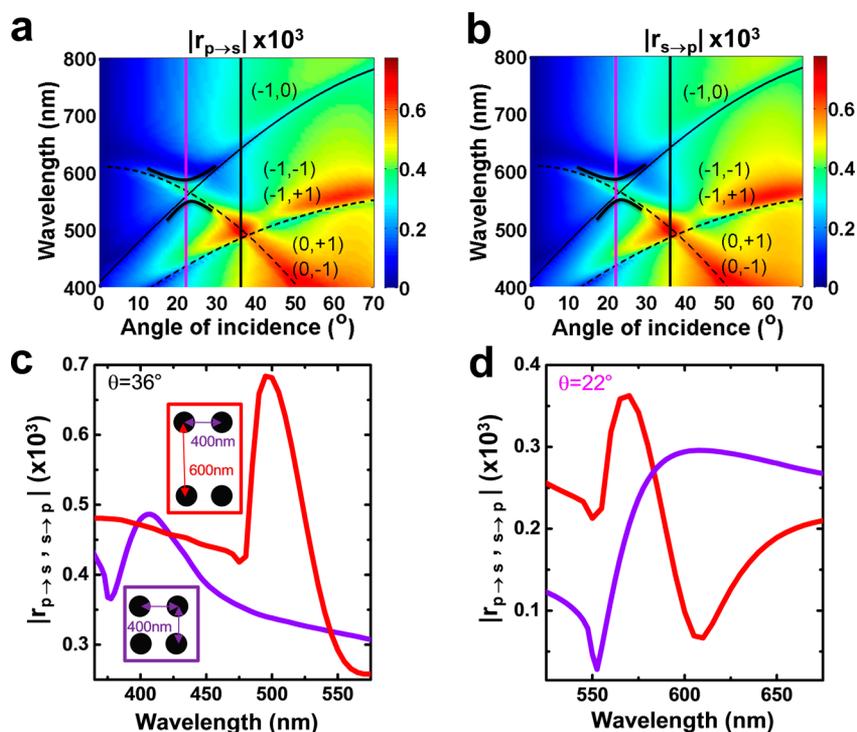
Figure 8. Calculated absolute values of the MO-induced polarization conversion reflection coefficients $r_{p\rightarrow s}$ (a) and $r_{s\rightarrow p}$ (b) of the rectangular 2D-MPC (400 nm × 600 nm) at $\phi = 0°$. Vertical lines indicate the angles of incidence 22° (pink line) and 36° (black line). The black thick lines at 22° at the intersection between the bands (−1,0) and (0, ±1) are guiding lines indicating a band gap opening. Calculated absolute values of $r_{p\rightarrow s,s\rightarrow p}$ of the rectangular (400 nm × 600 nm, red lines) and square (400 nm × 400 nm, violet lines) 2D-MPC at $\phi = 0°$ for $\theta = 36°$ (c) and for $\theta = 22°$ (d).

tion, Figures S5a, b) of the MO-induced polarization conversion coefficients $r_{s\rightarrow p}$ and $r_{p\rightarrow s}$ are *totally* independent of the polarization of the incident light and contain signatures of all the SPP modes excitable in the explored wavelength range, in complete agreement with the physical picture disclosed above.

We then come to the most interesting result of our study, namely, the observed large enhancement of the MOA at $\phi = 45°$ in correspondence of the excitation of the degenerate coupled modes originating from the noncollinear SPP waves (−1,0) and (0,−1). In this special case, the simultaneous availability of two SPP coupled modes, resonantly excited directly by the incident light with both s and p incident light and through the MO-induced polarization conversion, is the key of the observed MOA enhancement. This appears clear when inspecting Figure 7b, which displays the spectra for $\phi = 45°$ and $\theta = 45°$ of the MO induced polarization conversion coefficients $|r_{s\rightarrow p,p\rightarrow s}|$ together with the calculated absolute values of the reflection coefficients $|r_{ss}|$ and $|r_{pp}|$. As for the previous case, also for $\phi = 45°$, the $r_{s\rightarrow p,p\rightarrow s}$ spectra, as well as their complete spectral intensity maps (Supporting Information, Figure S5c,d), are identical, demonstrating once more that the MOA intensity difference between p and s polarizations is due to the pure optical reflectivity intensity difference. To summarize, the key message emerging from the physical picture disclosed above is that the enhancement of the L-MOKE MOA is possible only when two (or more) channels are available for direct and MO-induced resonant coupling of the incidence light to SPP modes and this is possible only when degenerate and noncollinear SPP coupled modes are involved.

Moreover, we envision that through plasmonic band engineering this MO-SPP-assisted polarization conversion can be further tuned by making more than two channels available,

namely designing the crystal lattice so that plasmonic bands can intersect at desired wavelengths and angles of incidence. As an illustrative example of the opportunities offered by such plasmonic band engineering, we consider an anisotropic 2D-MPC having a rectangular crystal lattice. The diameter of the holes considered in the simulations is the same as for the square lattice studied above.

Using a rectangular array with lattice parameters 400 nm × 600 nm and for $\phi = 0°$, an intersection between the two noncollinear bands (0, ± 1) and (−1, ±1) is produced at $\theta \approx 36°$ and at a wavelength of ~500 nm, while a second intersection between the collinear band (−1,0) and the noncollinear bands (0, ±1) is obtained at $\theta = 22°$ and 575 nm of wavelength (see Figure 8a,b). In Figure 8c we show the comparison between the calculated $r_{s\rightarrow p,p\rightarrow s}$ spectra at $\theta \approx 36°$ for the square (violet solid line) and rectangular (red solid line) lattices. In the case of the square lattice, the peak at ~400 nm corresponds to the enhancement of the polarization conversion effect due to the resonant excitation of the coupled SPP modes in the (−1, ±1) noncollinear bands (see Figure 6a). The intense peak at ~500 nm in the spectrum for the rectangular lattice is now produced by the resonant excitation of coupled SPP modes in the (−1, ±1) and (0, ±1) noncollinear bands. For the rectangular array, the enhancement of the polarization conversion is about two times that occurring in the square array as a consequence of the fact that now the channels for polarization conversion have been doubled. Therefore, the spectra in Figure 8c corroborate the physical picture put forward above and demonstrate that through plasmonic band engineering enhancement of the plasmon-assisted polarization conversion can be further strengthened by making more than two channels available for direct and MO-induced resonant coupling of the incidence light to SPP modes.

The spectrum of the calculated $r_{s \to p, p \to s}$ for the rectangular lattice that results from the other type of band intersection occurring at $\theta = 22°$ is shown in Figure 8d (red solid line). Also in this case, the spectrum at the same θ calculated for the square array is displayed (violet solid line) for comparison. For the square lattice, the broad maximum in the spectral range 550−650 nm arises from the resonant excitation of the mode in the collinear band (−1,0) (the sharp dip at 550 nm is due to the Rayleigh anomaly). For the rectangular lattice, the broad peak is replaced by a narrower and more intense peak at around 565 nm immediately followed by a dip at around 610 nm, yielding to a sort of symmetric resonant-antiresonant line shape. The effects of the plasmonic bands crossing, namely the increase of the channels available for direct and MO-induced resonant coupling of the incidence light to SPP modes, on the $r_{s \to p, p \to s}$ spectral behavior is, thus, now completely different with respect to the previous case shown in Figure 8a. We can conclude that when a plasmonic band crossing is produced, SPP modes interfere constructively when they have the same nature (case for $\theta \approx 36°$), while the interference is changing from constructive to destructive upon varying the wavelength when they are of different nature (case for $\theta = 22°$). In this respect, it is worth mentioning that in nonmagnetic rectangular 2D-PC, the intersection between collinear and noncollinear bands was experimentally observed to give rise to intriguing interference effects such as band gaps opening with the appearance of peculiar coupled SPP modes with a low group velocity and high radiative damping.[9] The complete spectral intensity maps of $r_{s \to p, p \to s}$ calculated for our rectangular lattice shown in Figure 8a,b indeed display that a clear band gap is opened by modes hybridization at the intersection of the two bands (see the black thick lines in the Figure 8a,b, indicating a band gap opening). We speculate here that the suppression of the polarization conversion effect at wavelengths around 610 nm might be due to the excitation of such coupled SPP modes with a low group velocity and high radiative damping. While further investigations are needed to confirm the origin of such intriguing behavior, on a more practical footing, the simulations clearly show that the coupling of such modes, which are different in nature, allows a fine-tuning of the polarization conversion effect in a sharp spectral region, opening the way to new avenues for plasmonic bands engineering of 2D-MPCs.

We finally mention that, in addition to the modification of the lattice parameters, one can also tune the MOA by playing with the holes diameter and shape. The detailed discussion of these effects is out of the scope of this work, but it is known that holes shape and dimensions can be tailored to tune the coupling efficiency between light and SPP modes and, as direct consequence, to further enhance and tune the MOA of the 2D-MPC.[23,36]

In summary, we have investigated a two-dimensional plasmonic crystal with a periodic array of cylindrical holes in a ferromagnetic layer, namely, a two-dimensional magneto-plasmonic crystal, supporting surface plasmon polariton modes displaying a two-dimensional plasmonic band structure. We have demonstrated that the intrinsic magneto-optical activity acting in the crystal plane allows an efficient coupling of the light to *all* the excitable surface plasmon polariton modes through the synergistic action between diffracting coupling and magneto-optical induced polarization conversion. This leads to the same magneto-optical response independently of the incident light polarization. We further demonstrated that a resonant enhancement of the magneto-optical response in

longitudinal Kerr configuration is induced when two or more channels are available for direct and magneto-optical induced resonant coupling of the incidence light to particular degenerate and *noncollinear* surface plasma polariton modes. The physics disclosed by our findings paves the way for the design of two-dimensional magnetoplasmonic crystals with tailored and enhanced magneto-optical response by engineering the plasmonic band structure via lattice design. In addition, two-dimensional magneto-plasmonic crystals offer the unique opportunity to explore other potential synergistic effects arising from peculiar static and dynamic magnetic configurations, such as periodic magnetic domains and spin waves displaying magnonic bands, that can be induced and controlled in this kind of system by an external magnetic field. For the sample studied here, we did not observe any clear effect on the magneto-optical activity spectra related to the nucleation of nonuniform magnetization states, like stripes domain structures that are known to occur at low magnetic field values (see Supporting Information, Figure S6). In the present sample, magnetic domains with magnetization oriented perpendicular to the saturation direction and with size comparable the holes diameter, that is, below 300 nm, are known to nucleate in form of stripes connecting the holes in the direction of the applied field.[37−40] According to Supporting Information, Figure S2, their size is, thus, always much smaller than the surface plasmon polariton propagation length for the sample studied here. We speculate that by making the holes bigger, namely the domains size bigger, we might expect to observe a field dependence of the magneto-optical activity spectra, which could increase further the potential of these magnetoplasmonics crystals. The concept of a two-dimensional magneto-plasmonic crystals controllable via an external magnetic field, with magnetically tunable resonant interaction effects between propagating magnetoplasmons, magnetostatic configurations, and perhaps even dynamic magnetization modes, opens up new perspectives toward an interplay between the fields of magnonics, spintronics, and plasmonics.[41]

■ METHODS

Optical and Magneto-Optical Characterization. The reflectivity spectra $(I_0 - I_R)/I_0$, where I_0 and I_R are the intensities of the incident and reflected light, respectively, were taken in the wavelength range 370−800 nm. The intensity of the light going directly to the detector was taken as the reference I_0 signal.

The wavelength dependence of the magneto-optical induced θ_K and ε_K (rotation and ellipticity polarization angles) of the reflected light, which define the MOA $= (\theta_K^2 + \varepsilon_K^2)^{1/2}$, were measured using a MOKE spectrometer working in longitudinal geometry in the wavelength range 440−800 nm. The incident light beam was linearly polarized with either *p*- or *s*-polarization. θ_K and ε_K were measured by switching the polarity of the magnetic field |H| = 2 kOe applied parallel to the crystal plane to activate the magneto-optical coupling in the constituent material. θ_K and ε_K were measured at each wavelength with the reflected beam passing through a photoelastic phase modulator and a polarizer before detection. Two lock-in amplifiers were used to filter the signals at the modulation frequency and at twice the modulation frequency in order to retrieve both quantities.[42]

Scattering-Matrix Method. All the calculations presented in this work have been carried out with a generalization of the scattering-matrix approach of Whittaker and Culshaw[43] that

some of us have recently developed.[34] This approach combines the scattering-matrix method with the Bloch theorem to describe both the optical and magneto-optical properties of arbitrary periodically patterned multilayered structures. In particular, this method is able to deal with MO configurations such as the longitudinal MOKE, which is out of the scope of other scattering-matrix approaches. Moreover, our method makes use of the so-called fast Fourier factorization, which allows for a very accurate convergence of the results upon increasing the number of plane waves used in the calculations. All the quantities shown in this work converged with an accuracy of 1% (relative error).

Fabrication Process. Large-area (4 mm × 4 mm) antidot structures were fabricated on commercially available silicon substrates using deep ultraviolet lithography at 248 nm exposing wavelength lithography followed by electron beam evaporation and lift-off processes. To create patterns in the resist, the substrate was coated with a 60 nm thick antireflective layer followed by a 480 nm positive deep UV photoresist, which is 4−5 times thicker than those used typically in electron beam lithography. This allows one to fabricate antidots with high aspect ratio and makes the lift-off process easier. A Nikon lithographic scanner with KrF excimer laser radiation was used to expose the resist. To convert the resist patterns into antidots, 80 nm thick Py layer was deposited using the electron beam evaporation technique at a rate of 0.02 nm s^{-1}. The pressure was maintained at about 2×10^{-6} Torr during the deposition at room temperature. Lift-off processing of the deposited film was carried out in isopropyl alcohol. More details of the processing steps can be found elsewhere.[32]

■ ASSOCIATED CONTENT

Ⓢ Supporting Information

The Supporting Information is available free of charge on the ACS Publications website at DOI: 10.1021/acsphotonics.5b00490.

> Dielectric function of permalloy. Dispersion relation and propagation length of surface plasmon polariton modes in permalloy continuous film. Experimental and calculated Kerr ellipticity and rotation of the 2D-MPC and of the continuous film for p-polarized light, $\phi = 45°$ and $\theta = 30°$. Calculated intensity maps of the ratio between the MOA of the 2D-MPC and that of the continuous Py film. Calculated absolute values of the MO-induced polarization conversion reflection coefficients of the 2D-MPC. Experimental MOA spectra measured at $\phi = 45°$ and $\theta = 30°$, for p- and s-polarized light at saturation and at |H| = 40 Oe (PDF).

■ AUTHOR INFORMATION

Corresponding Author

*E-mail: p.vavassori@nanogune.eu.

Present Address

⊥Western Digital, 1710 Automation Pkwy, San Jose, CA 95131, United States (D.T.).

Notes

The authors declare no competing financial interest.

■ ACKNOWLEDGMENTS

■ REFERENCES

(1) Raether, H. Surface Plasmons on Smooth and Rough Surfaces and on Gratings. *Springer Tracts in Modern Physics*; Springer: New York, 1988.

(2) Meyer, S.*Plasmonics: Fundamental and Applications*; Springer: New York, 2007.

(3) Ritchie, R. H.; Arakawa, E. T.; Cowan, J. J.; Hamm, R. N. Surface-Plasmon Resonance Effect in Grating Diffraction. *Phys. Rev. Lett.* **1968**, *21*, 1530−1533.

(4) Watts, R. A.; Preist, T. W.; Sambles, J. R. Sharp Surface-Plasmon Resonances on Deep Diffraction Gratings. *Phys. Rev. Lett.* **1997**, *79*, 3978−3981.

(5) Kats, A. V.; Nesterov, M. L.; Nikitin, A. Yu. Excitation of Surface Plasmon-Polaritons in Metal Films with Double Periodic Modulation: Anomalous Optical Effects. *Phys. Rev. B: Condens. Matter Mater. Phys.* **2007**, *76*, 045413.

(6) Romanato, F.; Lee, K. H.; Ruffato, G.; Wong, C. C. The Role of Polarization on Surface Plasmon-Polariton Excitation on Metallic Gratings in the Conical Mounting. *Appl. Phys. Lett.* **2010**, *96*, 111103.

(7) Sapozhnikov, M. V.; Gusev, S. A.; Troitskii, B. B.; Khokhlova, L. V. Optical and Magneto-Optical Resonances in Nanocorrugated Ferromagnetic Films. *Opt. Lett.* **2011**, *36*, 4197−4199.

(8) Kang, H. K.; Lee, K. H.; Wu, Y.; Wong, C. C. The Role of Polarization on 2D Plasmonic Crystals. *Plasmonics* **2011**, *6*, 373−380.

(9) Billaudeau, C.; Collin, S.; Sauvan, C.; Bardou, N.; Pardo, F.; Pelouard, J.-L. Angle-Resolved Transmission Measurements through Anisotropic Two-Dimensional Plasmonic Crystals. *Opt. Lett.* **2008**, *33*, 165−167.

(10) Ebbesen, T. W.; Lezec, H. J.; Ghaemi, H. F.; Thio, T.; Wolff, P. A. Extraordinary Optical Transmission through Sub-Wavelength Hole Arrays. *Nature* **1998**, *391*, 667−669.

(11) García-Vidal, F. J.; Martín-Moreno, L.; Ebbesen, T. W.; Kuipers, L. Light Passing Through Subwavelength Apertures. *Rev. Mod. Phys.* **2010**, *82*, 729−787.

(12) Altug, H.; Englund, D.; Vuckovic, J. Ultrafast Photonic Crystal Nanocavity laser. *Nat. Phys.* **2006**, *2*, 484−488.

(13) Bozhevolnyi, S. I.; Volkov, V. S.; Devaux, E.; Laluet, J.-Y.; Ebbesen, T. W. Channel Plasmon Subwavelength Waveguide Components Including Interferometers and Ring Resonators. *Nature* **2006**, *440*, 508−511.

(14) Lal, S.; Link, S.; Halas, N. J. Nano-Optics from Sensing to Waveguiding. *Nat. Photonics* **2007**, *1*, 641−648.

(15) Ferry, V. E.; Sweatlock, L. A.; Pacifici, D.; Atwater, H. A. Plasmonic Nanostructures Design for Efficient Light Coupling into Solar Cells. *Nano Lett.* **2008**, *8*, 4391−4397.

(16) Maccaferri, N.; et al. Tuning the Magneto-Optical Response of Nanosize Ferromagnetic Ni Disks Using the Phase of Localized Plasmons. *Phys. Rev. Lett.* **2013**, *111*, 167401.

(17) Armelles, G.; Cebollada, A.; García-Martín, A.; González, M. U.; García, F.; Meneses-Rodríguez, D.; de Sousa, N.; Pérez-Froufe, L. S. Mimicking Electromagnetically Induced Transparency in the Magneto-Optical Activity of Magnetoplasmonic Nanoresonators. *Opt. Express* **2013**, *21*, 27356−27370.

(18) Maccaferri, N.; Kataja, M.; Bonanni, V.; Bonetti, S.; Pirzadeh, Z.; Dmitriev, A.; van Dijken, S.; Åkerman, J.; Vavassori, P. Effects of a Non-Absorbing Substrate on the Magneto-Optical Kerr Response of

Plasmonic Ferromagnetic Nanodisks. *Phys. Status Solidi A* **2014**, *211*, 1067−1075.

(19) Maccaferri, N.; Gregorczyk, K. E.; de Oliveira, T. V. A. G.; Kataja, M.; van Dijken, S.; Pirzadeh, Z.; Dmitriev, A.; Åkerman, J.; Knez, M.; Vavassori, P. Ultrasensitive and label-free molecular-level detection enabled by light phase control in magnetoplasmonic nanoantennas. *Nat. Commun.* **2015**, *6*, 6150.

(20) Zubritskaya, I.; Lodewijks, K.; Maccaferri, N.; Mekonnen; Dumas, R. K.; Åkerman, J.; Vavassori, P.; Dmitriev, A. Active magnetoplasmonic ruler. *Nano Lett.* **2015**, *15*, 3204−3211.

(21) Lodewijks, K.; Maccaferri, N.; Pakizeh, T.; Dumas, R. K.; Zubritskaya, I.; Åkerman, J.; Vavassori, P.; Dmitriev, A. Magneto-plasmonic Design Rules for Active Magneto-Optics. *Nano Lett.* **2014**, *14*, 7207−7214.

(22) Cistis, G.; Papaioannou, E.; Patoka, P.; Gutek, J.; Fumagalli, P.; Giersing, M. Optical and Magnetic Properties of Hexagonal Arrays of Subwavelength Holes in Optically This Cobalt Films. *Nano Lett.* **2009**, *9*, 1−6.

(23) Fang, H.; Caballero, B.; Akinoglu, E. M.; Papaioannou, E. Th.; García-Martín, A.; Cuevas, J. C.; Giersig, M.; Fumagalli, P. Observation of Hole-Size-Dependent Energy Shift of the Surface-Plasmon Resonance in Ni Antidot Thin Films. *Appl. Phys. Lett.* **2015**, *106*, 153104.

(24) Armelles, G.; Caballero, B.; Cebollada, A.; Garcia-Martin, A.; Meneses-Rodríguez, D. Magnetic Field Modification of Optical Magnetic Dipoles. *Nano Lett.* **2015**, *15*, 2045−2049.

(25) Chetvertukhin, A. V.; Grunin, A. A.; Baryshev, A. V.; Dolgova, T. V.; Uchida, H.; Inoue, M.; Fedyanin, A. A. Magneto-Optical Kerr Effect Enhancement at the Wood's Anomaly in Magnetoplasmonic crystals. *J. Magn. Magn. Mater.* **2012**, *324*, 3516−3518.

(26) Kostylev, N.; Maksymov, I. S.; Adeyeye, A. O.; Samarin, S.; Kostylev, M.; Williams, J. F. Plasmon-assisted High Reflectivity and Strong Magneto-Optical Kerr Effect in Permalloy Gratings. *Appl. Phys. Lett.* **2013**, *102*, 121907.

(27) Newman, D. M.; Wears, M. L.; Matelon, R. J.; Hooper, I. R. Magneto-Optic Behaviour in the Presence of Surface Plasmons. *J. Phys.: Condens. Matter* **2008**, *20*, 345230.

(28) Papaioannou, E. Th.; et al. Magneto-Optics Enhancement and Magnetic Properties in Fe Antidot Films with Hexagonal Symmetry. *Phys. Rev. B: Condens. Matter Mater. Phys.* **2010**, *81*, 054424.

(29) Torrado, J. F.; Papaioannou, E.Th.; Ctistis, G.; Patoka, P.; Giersig, M.; Armelles, G.; García-Martín, A. Plasmon Induced Modification of the Transverse Magneto-Optical Response in Fe Antidot arrays. *Phys. Status Solidi RRL* **2010**, *4*, 271−273.

(30) Melander, E.; Östman, E.; Keller, J.; Schmidt, J.; Papaioannou, E. Th.; Kapalis, V.; Arnalds, U. B.; Caballero, B.; García-Martín, A.; Cuevas, J. C.; Hjörvarsson, B. Influence of the Magnetic Field on the Plasmonic Properties of Transparent Ni Anti-Dot Arrays. *Appl. Phys. Lett.* **2012**, *101*, 063107.

(31) Xia, W. B.; et al. Optical and Magneto-Optical Anisotropies in Large-Area Two-Dimensional Co Antidots Film. *Opt. Express* **2014**, *22*, 1359−1365.

(32) Adeyeye, A. O.; Singh, N. Large Area Patterned Magnetic Nanostructures. *J. Phys. D: Appl. Phys.* **2008**, *41*, 153001.

(33) Freiser, M. A Survey of Magnetooptic Effects. *IEEE Trans. Magn.* **1968**, *4*, 152−161.

(34) Caballero, B.; García-Martín, A.; Cuevas, J. C. Generalized Scattering-Matrix Approach for Magneto-Optics in Periodically Patterned Multilayer Systems. *Phys. Rev. B: Condens. Matter Mater. Phys.* **2012**, *85*, 245103.

(35) Neuber, G.; et al. Temperature-Dependent Spectral Generalized Magneto-Optical Ellipsometry. *Appl. Phys. Lett.* **2003**, *83*, 4509−4511.

(36) Koerkamp, K. J. K.; Enoch, S.; Segerink, F. B.; van Hulst, N. F.; Kuipers, L. Strong Influence of Hole Shape on Extraordinary Transmission through Periodic Arrays of Subwavelngth Holes. *Phys. Rev. Lett.* **2004**, *92*, 183901.

(37) Guedes, I.; et al. Magnetization of Negative Magnetic Arrays: Elliptical Holes on a Square Lattice. *Phys. Rev. B: Condens. Matter Mater. Phys.* **2000**, *62*, 11719.

(38) Vavassori, P.; Gubbiotti, G.; Zangari, G.; Yu, C. T.; Yin, H.; Jiang, H.; Mankey, G. J. Lattice Symmetry and Magnetization Reversal in Micron-Size Antidot Arrays in Permalloy Film. *J. Appl. Phys.* **2002**, *91*, 7992.

(39) Guedes, I.; et al. Magnetization Reversal in a Fe Film with an Array of Elliptical Holes on a Square Lattice. *Phys. Rev. B: Condens. Matter Mater. Phys.* **2003**, *67*, 024428.

(40) Guedes, I.; et al. Domain Formation in Arrays of Square Holes in a Fe Film. *Phys. Rev. B: Condens. Matter Mater. Phys.* **2002**, *66*, 014434.

(41) Maksymov, I. S. Magneto-Plasmonics and Resonant Interaction of Light with Dynamic Magnetisation in Metallic and All-Magneto-Dielectric Nanostructures. *Nanomaterials* **2015**, *5*, 577.

(42) Vavassori, P. Polarization Modulation Technique for Magneto-Optical Quantitative Vector Magnetometry. *Appl. Phys. Lett.* **2000**, *77*, 1605−1607.

(43) Whittaker, D.; Culshaw, I. Scattering-Matrix Treatment of Patterned Multilayer Photonic Structures. *Phys. Rev. B: Condens. Matter Mater. Phys.* **1999**, *60*, 2610−2618.